TiO 2 –SiO 2 nanocomposite thin films deposited by direct liquid injection of colloidal solution in an O 2 /HMDSO low-pressure plasma

Maria Mitronika, Jacopo Profili, Antoine Goullet, Nicolas Gautier, Nicolas Stephant, Luc Stafford, Agnès Granier, Mireille Richard-Plouet

TiO_2-SiO_2 Nanocomposite thin films deposited by Direct Liquid Injection of colloidal solution in an O_2/HMDSO low-pressure plasma

Maria Mitronika[1], *Jacopo Profili*[2], *Antoine Goullet*[1], *Nicolas Gautier*[1], *Nicolas Stephant*[1], *Luc Stafford*[2], *Agnès Granier*[1], *Mireille Richard-Plouet*[1*]

[1] Université de Nantes, CNRS, Institut des Matériaux Jean Rouxel, IMN, F-44000 Nantes, France

[2] Département de physique, Université de Montréal, 1375 Avenue Thérèse-Lavoie-Roux, Montréal, Québec, H2V 0B3, Canada

[*]corresponding author: Mireille.Richard@cnrs-imn.fr

Keywords: low-pressure plasma processing, direct-liquid injection, colloidal solution, TiO_2 nanoparticles, TiO_2-SiO_2 nanocomposite thin films

Abstract: TiO_2 nanoparticles (NPs), 3 nm in size, were injected inside a very-low-pressure O_2 plasma reactor using a liquid injector and following an iterative injection sequence. Simultaneously, hexamethyldisiloxane (HMDSO) vapor precursor was added to create a SiO_2 matrix and a TiO_2-SiO_2 nanocomposite (NC) thin film. Both the liquid injection and vapor precursor parameters were established to address the main challenges observed when creating NCs. In contrast to most aerosol-assisted plasma deposition processes, Scanning/Transmission Electron Microscopy (S/TEM) indicated isolated (i.e. non-agglomerated) NPs distributed in a rather uniform way in the matrix. The fraction of the TiO_2 NPs inside the SiO_2 matrix was estimated by SEM, Spectroscopic Ellipsometry (SE), and X-ray Photoelectron Spectroscopy. All techniques provided coherent values, with percentages between 12 and 19%. Despite the presence of TiO_2 NPs, SE measurements confirmed that the plasma-deposited SiO_2 matrix was dense with an optical quality similar to the one of thermal silica. Finally, the percentage of TiO_2 NPs inside the SiO_2 matrix and the effective refractive index of the NCs can be tuned through judicious control of the injection sequence.

1. Introduction

Nowadays, there is an ongoing demand for smaller, faster, and low-cost integrated systems. Achieving this often requires new materials and structures that combine the more conventional ones. In this context, nanocomposite (NC) thin films formed of nanoobjects embedded in a matrix have gained great attention, as the properties of the resulting composite may be more likely to resemble those of the interface zones rather than those of the original constituents[1]. The high surface-area-to-volume ratio in NCs can also lead to enhanced macroscopic properties compared to the bulk materials.

One of the most significant challenge in the development of NC thin films is the control of the growth mechanisms, the final morphology and the incorporation of the nanoobjects using reproducible, versatile and low-cost processes. Several chemical and physical methods have been used in recent years. For example, sol-gel is a well-established process based on hydrolysis and condensation reactions.[2,3] The main drawback of this approach is the need of several steps to produce NC thin films. In addition, the toxicity of the nanoparticles (NPs) during the drying of the film[4] limits the industrialization. Vacuum processes such as PECVD or CVD have also demonstrated their ability to synthesize NC thin films by controlling the plasma- or thermally-activated reaction pathways.[5,6] In parallel, sputtering approaches have also been used to create metal, metal-oxide or metal-nitrides NC thin films. [4,7]

Recently, there have been some attempts using hybrid (aerosol-assisted, direct liquid injection etc.) approaches for the creation of NC thin films. Profili et al. [8] implemented a one-step approach for the deposition of ZnO-SiO_2 NC coatings on wood by the atomization of a stable suspension of ZnO dispersed in hexamethyldisiloxane (HMDSO) in an atmospheric pressure dielectric barrier discharge (DBD). Ross et al.[9] elaborated composite films using an ultrasonic atomizer and a PECVD system using Tetraethoxysilane (TEOS) as a matrix precursor and polystyrene nanoparticles with a mean size of 96 nm. The pressure in the specific system was varied between 100 and 500 mTorr. More recently, Kahn et al.[10] proposed a new method that allowed to synthesize NPs from organometallic precursor in a reactor-injector prior to their injection in a RF low-pressure plasma reactor at 750 mTorr. The resulted NC thin films consisted of small (6 ± 3 nm) and isolated ZnO NPs homogeneously dispersed in an amorphous hydrogenated carbon matrix. This increased interest in hybrid approaches led to the development of new direct liquid injection systems[11] and studies regarding the interactions of the liquid droplets with the low pressure plasma systems [12] (misty plasmas). As a general trend, most of these studies focus on the deposition of inorganic NPs-organic matrix NC film. The majority of the reposted works involve high-pressure and atmospheric-pressure plasma system. These systems have been thoroughly studied mainly because of the technically-challenging conditions existing at very low pressures (*e.g.* risk of contamination of the vacuum chamber, malfunction of the turbomolecular pump, fast liquid vaporization without reaching the substrate).[13,14] In most cases, however, the NPs in NC thin films are agglomerated, and their size is increased compared to the one in the colloidal solution before their injection in the plasma. [13,15–22]

The main bottlenecks for producing NC thin films are incorporating a high-volume fraction, preventing the agglomeration of NPs and dispersing them homogeneously in the matrix. Using a very-low-pressure system, the objective is to deposit thin films incorporating 3-nm TiO_2 NPs in a high-quality inorganic SiO_2 matrix. This is accomplished by the direct liquid injection of the 3-nm TiO_2 NPs colloidal solution without a carrier gas and the addition of HMDSO vapor precursor in the very-low-pressure O_2 plasma. Furthermore, as several works involving atmospheric-pressure plasma systems reported challenges to deposit in one-step and acquire good quality NC films, the differences and prospects in using very-low-pressure hybrid systems is investigated. The evaluation of the NC's quality, homogeneity and distribution of the TiO_2 NPs are achieved by various characterization techniques such as high-resolution Scanning Transmission Electron Microscopy (HR-STEM), Energy Dispersive X-ray spectrometry (EDX), Atomic Force microscopy (AFM) and X-ray photoelectron spectroscopy (XPS). Finally, with this work, besides establishing this novel and versatile approach, the objective is to identify experimental conditions for acquiring thin films oriented towards optical applications. Therefore, the optical characteristics of the film, such as its effective refractive index, are being extracted with Spectroscopic Ellipsometry (SE).

2. Experimental Details

2.1 TiO_2 NPs colloidal solution

The colloidal solution used for the injection of the TiO_2 NPs in the very-low-pressure plasma has been synthesized following a specific protocol developed at the Institut des Matériaux Jean Rouxel.[23,24] The NPs enclosed in the colloidal solution were well-defined and monodispersed with an anatase crystalline structure. Their mean hydrodynamic diameter (including species of the solvent surrounding the NPs to counterbalance surface charge) obtained by Dynamic Light Scattering (DLS) with Zetasizer NanoZS (Malvern) was centered on 3.7 nm (Figure 1). The double layer surrounding the NPs has been estimated at 1 nm.[24] Therefore, the actual TiO_2 nanocrystallite diameter lay at 2.7 nm. As synthesized, the solvent of this solution was a mixture of 4-methyl-1,3-dioxolan-2-one also known as propylene carbonate (PC) and 1,2-propanediol or propylene glycol (PG), with a molar fraction of 27%:73% respectively. From previous studies of our group [23,25], we identified that some solvent molecules remain attached to the surface of the NPs, creating an 4.7 Å hydroxylated and organic shell around TiO_2 NPs.

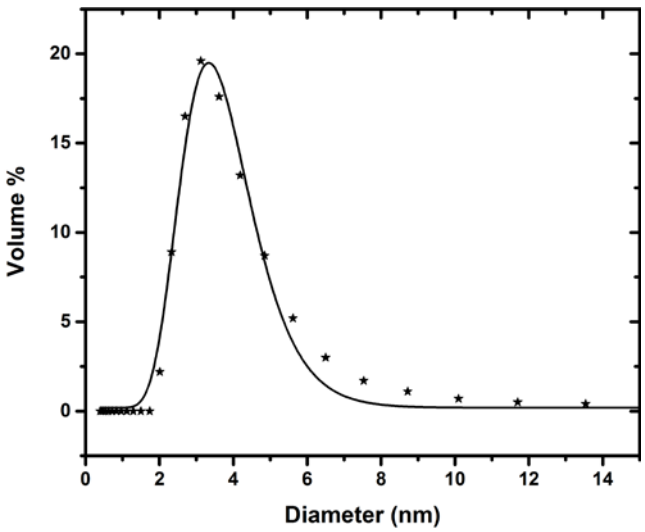

Figure 1: Hydrodynamic size distribution of the TiO_2 NPs inside the as-prepared (PC-PG) colloidal solution deduced from DLS. Line corresponds to a Log-Normal distribution fit, based on which the mean diameter size was extracted.

For the effective injection and evaporation of the colloidal solution in the very-low-pressure PECVD system, the dilution of the colloidal solution with a more volatile one was carried out. Therefore, the final colloidal solution used was a mixture of PC:PG:Methanol with a volume fraction of 20.25:54.75:25 . The size distribution of TiO_2 NPs in the diluted solution was verified with DLS and was not altered by either dilution or long-time storage..

2.2 Deposition of TiO_2-SiO_2 NC thin films using the hybrid approach

For the elaboration of the TiO_2-SiO_2 NC thin film, the colloidal solution was injected in a very-low-pressure PECVD reactor. The schematic representation of the hybrid experimental setup is given in Figure 2. The reactor comprises a very-low-pressure high-density Inductively Coupled Plasma (ICP) source created at 13.56 MHz (400 W) in a fused silica discharge tube using a helicon antenna which is also connected to a matching network. A static magnetic field (50 G) is applied to the source in order to confine the electrons and densify the plasma. The plasma then expands into a stainless-steel processing chamber where the substrate holder is located. The substrate holder is 17 cm in diameter located in the middle of the processing chamber with a distance of 16.8 cm from the bottom of the ICP antenna. The Si substrates used, which were positioned in the middle of the substrate holder, were 1 cm x 2 cm in dimension and their temperature was measured at 400 K through temperature-sensitive labels located at the substrate's backside. In this system, plasma gases (95% O_2, 5% Ar here) are introduced at the top of the plasma source and the high-vacuum pumping system is located 11 cm from the bottom of the processing chamber. The outlet of the vacuum pumping system that includes also a cold trap, is 10 cm in diameter. In Figure 2b, its location related to the substrate holder and the liquid doser can be seen. More information about the reactor can be found in [26,27].

For the deposition of the SiO_2 matrix, HMDSO vapor was introduced from a heated-container (at 35.8 °C) without any carrier gas through a distribution ring (indicated with blue in Figure 2), located 8 cm above the substrate. The injection of the TiO_2 colloidal solution was

achieved through a separate industrial direct-liquid doser (indicated with red in Figure 2). It is an injection system from Kemstream that features a normally closed fast solenoid valve (or injector), with a small conductance (flow coefficient), commonly called Cv. This valve is controlled in pulsed regime. The orifice of the injection system includes 8 holes with a diameter of 70 µm each. This injection system was mounted on the PECVD reactor with an angle of 55° with respect to the substrate holder. The distance of the injector to the reactor was fixed at 20 cm and therefore the distance of the injector to the substrate can be calculated at 48.24 cm. The pipe connecting the injector to the reactor was heated (yellow lines indicating the heating wire in Figure 2) at 423 K to enhance the evaporation process of the produced droplets.

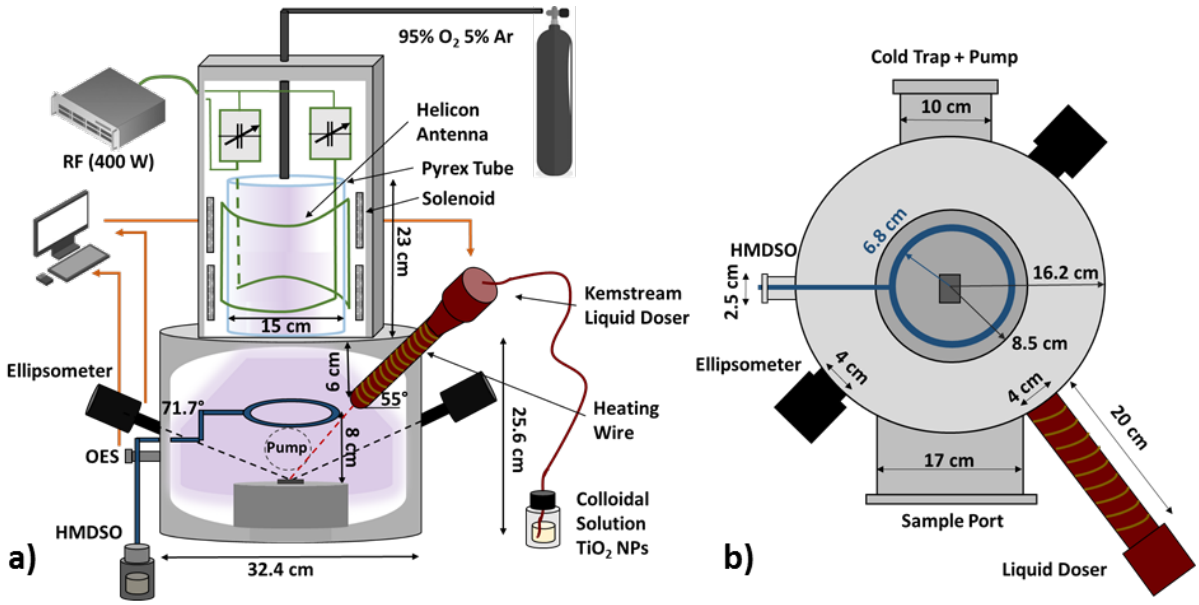

Figure 2: Schematic of the hybrid experimental setup including the low pressure ICP O_2 reactor, the liquid doser apparatus (with red) and the HMDSO vapor distribution system (with bleu) at a) side view and b) top view. The *in situ* characterization techniques are also indicated on this schematic.

For maintaining very-low pressure during the deposition (3 mTorr) and therefore obtaining a high-quality inorganic matrix, no additional carrier gas has been used to assist the injection of TiO_2 NPs. In such conditions, the droplet creation and the formation of the aerosol were mainly driven by the difference in pressure between the reservoir of the colloidal solution (760 Torr) and the plasma reactor (3 mTorr).[28] For this specific pressure difference, the mean droplet size obtained by Phase Doppler Anemometry (PDA) was 65.0 µm with a standard deviation of 29 µm. The opening of the injection valve was trigged by applying a positive pulse controlled by the VapSoft software of the direct-liquid injector. It is worth highlighting that during each pulsed injection of the colloidal solution in the plasma reactor the pressure instantaneously increased from 3 to 15 mTorr due to solvent evaporation[12] and then returned back to the steady-state pressure (3 mTorr) within less than 2 s. The pressure variation was detected from the capacitance diaphragm gauge (MKS Instruments France SA) and was read on the go. Additionally, the 15 mTorr was the maximum value that was provided by the gauge reading. Upon injection and pressure increase, the intensity of the ICP O_2 plasma is decreased retrieving within less than 2 seconds its usual brightness. Despite this fact, the plasma is never

extinguished remaining ignited during the total duration of the process. As a matter of fact, the intensities of O and Ar lines (at 394.5 nm and 419.8 nm, respectively) measured by time resolved OES are supplied as Electronic Supporting Information (ESI). These results, indicate that during each injection (within the DLI-ON), the emission intensities of the Ar and O lines are decreased trying to retrieve their steady state value within the pulses (Figure S1). This variation, especially for the Ar emission intensity is related to the pressure variation. Both intensities never reach a zero value verifying once more that the plasma remains ignited during the total duration of the hybrid deposition process. Regarding the RF power supply, during the droplet injection, a reflected power with a mean value of 2 W is provided by the CESAR RF Power Generator.

For deposition experiments, the total sequence length was set at one minute (Figure 2). More specifically, during the first 20 s, N=10 pulses of 1 ms (T_{ON} =1 ms) were triggered each two seconds (T=2 s). Thus, after this first-time lapse of N*2 s = 20 s, the valve remained closed for 60-N*2 s = 40 s (T_{OFF}). Such sequence was repeated for 50 minutes. The solvent mass rate was estimated at 2.33 mg per pulsed injection and therefore 23.3 mg per minute for N=10 cycles. During this intermittent mode of injection (Figure 3), the oxygen mass flow rate of the working gas was set at 24 SCCM (standard cubic centimeters per minute) while the continuous mass flow rate of HMDSO vapor was maintained at 0.11 SCCM. The fraction between HMDSO and O_2 was chosen in a way to produce a silica-like matrix with a very low carbon content[29]. O_2 was also used to ensure the removal of solvent-based organic moieties surrounding TiO_2 NPs[30].

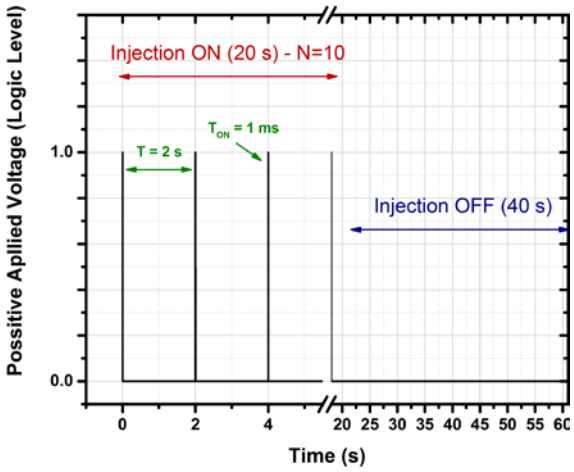

Figure 3: Description of the plasma deposition sequence including the first part of pulsed injection of the colloidal solution (10 cycles of T_{ON} with an off time of 2 s between each pulse for a total of 20 s) and the second part without liquid injection (for a total off time T_{OFF} = 40s).

2.3 Characterization of the NC thin films

The cross section and distribution of the TiO_2 NPs inside the SiO_2 matrix were investigated (Figure 4 a, b ,c) using transmission electron microscopy (S/TEM Themis Z G3, 300kV, Thermo Fisher Scientific). A typical image of high-angle annular dark-field scanning transmission electron microscopy (HAADF-STEM, 28.5 mrad, probe corrected) is reported in

Figure 4 d. The elemental mapping (Figure 4 e f g) was performed using EDX (energy dispersive X-ray spectrometer) analysis. For the effective characterization of the samples through TEM, the deposition was carried on Tin doped Indium oxide deposited on polyethylene terephthalate (ITO (50 nm) / PET (125 µm), Sheldahl). Cross-sections of the sample were prepared by using an ultramicrotome (Leica UC7/FC7) equipped with diamond knife (Diatome). The morphological analysis of the TiO_2-SiO_2 NC film on Si was carried out through Scanning Electron Microscopy (SEM) with a JEOL JSM 7600F, in a secondary electron mode, operating at 5 kV. The chemical analysis by EDX was conducted with a SAMx SDD system on a SEM JEOL JSM 5800LV. To increase the EDX signals, a dedicated thicker film was prepared (224 nm). To ensure that no additional Si coming from the substrate would interfere with the quantification of the silica matrix the dedicated thicker NC film was deposited on ITO/PET substrate. To probe different thicknesses, EDX spectra were recorded at three accelerating voltages: 15 kV, 10 kV and 7 kV and a magnification of X1000 (2552 μm^2) was chosen to smooth any local anomalies of chemical concentrations. The software Stratagem was used for EDX measurements because first the volume irradiated by the electron beam and second the X-ray collected are related to a larger depth than the thickness of the top layer. [31] The atomic percentages were determined by considering a theoretical model for the probed zone [32]. For this, three layers were considered: first, 224 nm of NC (Ti, Si, O), second, 50 nm of ITO (In, Sn, O), and third, PET (C, O). The different atomic percentages were fitted to reproduce the intensity of EDX signals as a function of the accelerating voltage, accounting for the thicknesses of the NC and ITO and attenuation of signals throughout the different layers. The determination of carbon and oxygen was not reliable because the corresponding signals may come from ITO and PET underneath (one must also consider that the effective thickness of PET analyzed by EDX depends on the accelerating voltage). However, the precautions taken before acquisition and the good fit between theoretical curves generated by Stratagem and experimental values make it possible to rely on the results concerning silicon and titanium atomic percentages.

The optical characteristics and composition of the TiO_2-SiO_2 NC thin films deposited on silicon substrates were also examined through a rotating compensator spectroscopic ellipsometer (J.A. Woollam M-2000). The measurements were conducted in situ (i.e. during plasma deposition) in the wavelength range of 245 to 1000 nm at 71.7° incident angle.

Atomic Force Microscopy (AFM) was used in tapping mode to investigate the nanostructured topography and roughness of the NC thin films. AFM Nanowizard II (JPK Instruments), Al-coated cantilever (PPP-NCHR-50 from NANOSENSORS) with a free resonance frequency of 330 kHz and a typical spring constant of about 42 N/m were used. The size distribution of the NPs was deduced from the AFM scans by using the ImageJ software after adjustment of the threshold and transformation in binary format.

Raman spectroscopy measurements were performed using a microconfocal Raman microscope (Renishaw inVia). The instrument was equipped with a double edge filter to eliminate the Rayleigh scattering and a charged couple device (CCD) camera working at a temperature of 220 K with a 1024x256 pixel array. The setup was composed of a confocal

microscope that was equipped with an automated XYZ table and an X50 magnification objective. The laser excitation source used was set at 514 nm and the focused power was adjusted to avoid any degradation of the samples. Therefore, the power was fixed at 1.5mW and a recording time of 1 s with an accumulation of 10 measurements was used.

The chemical characterization of the topmost surface was investigated with X-ray photoelectron spectroscopy (XPS) on a Kratos Nova spectrometer with Al Kα radiation at 1486.6 eV. Neutralization of the surface was applied to avoid differential charging effect. Survey spectra were measured from 1200 to -2 eV (Binding Energy) using a pass energy of 160 eV whereas high-resolution spectra over specific regions of interest were recorded with a pass energy of 40 eV. Short time measurements were recorded (dwell of 100 ms per 0.1 eV step-scan for O1s, Ti 2p and 200 ms for C1s). After checking that no X-ray damage was induced, the scans were summed up to increase the signal-to-noise ratio. The decomposition and fitting of the measured XPS peaks was carried out using CasaXPS software [33]. After accounting for the background using a U2-Tougaard background, Gaussian-Lorentzian (30-70%) functions were selected to model the different components. The signals were calibrated in energy according to the position of the C 1s band at the binding energy of 285 eV.

To be able to compare the results obtained from different characterization techniques, detailed calculations have been achieved (which are supplied as Electronic Supporting Information) to transform at% of elements to vol% of oxides.

3. Results

3.1 Structural characterization of the TiO_2-SiO_2 NC thin films

Cross section structural analysis of the plasma-deposited NC thin film was performed using TEM and STEM (Figure 4). Through multiple measurements on low magnification images (Fig. 4a), the thickness of the film was estimated at 85 +/- 6 nm (a growth rate of 1.7 nm/min for a total plasma deposition time of 50 min). This value is comparable to the one achieved in O_2/HMDSO plasmas without injection of the TiO_2 colloidal solution[29]. Using high-resolution images on the rectangular area (black contour) shown in Fig. 4b and based on the contrast between the amorphous matrix and the basal planes of the nanocrystals, some TiO_2 NPs can be identified (enlarged NPs as an inset in Figure 4) and stressed with white-rounded contour shapes (Figure 4c). Interestingly, no agglomeration of these NPs is observed but rather an assembly of small and isolated TiO_2 NPs in the SiO_2 matrix. Using ImageJ software, the size of each of these NPs (14 nanoparticles identified in the specific zone probed by electron microscopy) was extracted and their mean value was found to be at 2.7 ± 0.4 nm. By comparing this value with the hydrodynamic diameter of TiO_2 NPs in the colloidal solution obtained by DLS (2.7 nm + 1 nm, Figure 1), it can be confirmed that the NPs' size remains intact following the aerosol formation and plasma deposition. This is a remarkable result with respect to other experiments on hybrid plasma deposition of NC thin films for which agglomeration phenomena were deemed unavoidable[13,15–22]. Moreover, TiO_2 NPs displayed in Figure 4c seem dispersed in a rather random way in the SiO_2 matrix, with no evidence of preferential

incorporation sites. No cracking of the SiO_2 layers is visible, showing that the insertion of the NPs does not strongly affect the growth of the silica layer.

The typical HAADF-STEM image given in the same figure confirms that no bright contrast associated to possible agglomeration of the electronically denser TiO_2 NPs is detected, indicating the homogeneity of the NPs dispersion, at this scale of observation. Moreover, EDX elemental mapping also confirms that both oxygen and silicon (Fig.4 e,f) are homogeneously distributed along the cross section of the NC thin film. On the other hand, Ti (Fig. 4g) signal, which is only linked to the TiO_2 NPs, is identified with some small dots verifying the TEM images (Fig. 4c) and their distribution inside the film. Since the data are a projection of 80 nm thin sample, the reinforcement in contrast, (in some small parts of Fig.4g) may come from particles distributed along this thickness.

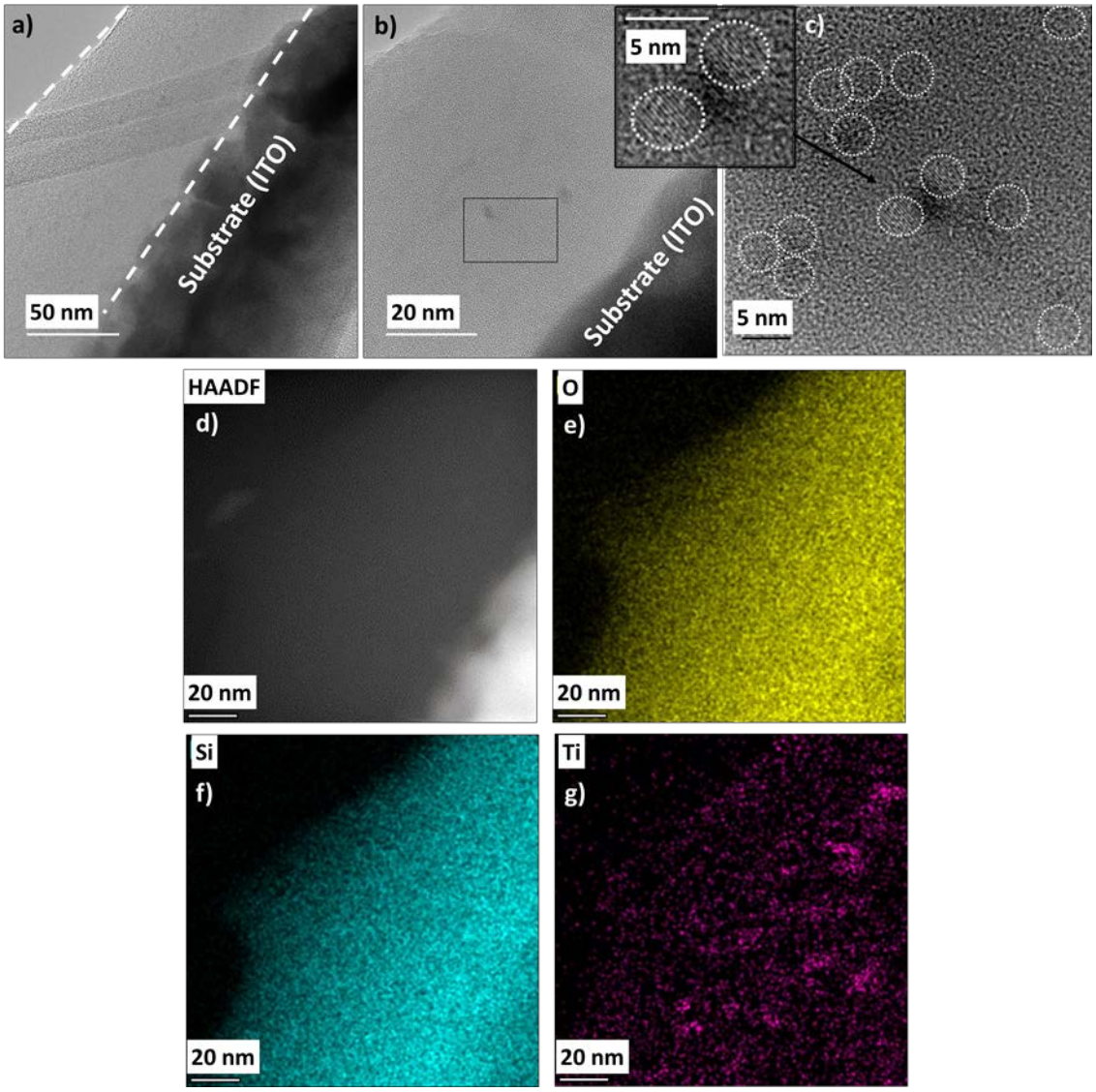

Figure 4: TEM cross section of the TiO_2-SiO_2 NC thin film a) in low magnification indicated with white dashed lines, b) high magnification and c) higher magnification image focusing on the distributed TiO_2 NPs inside the SiO_2 matrix. An inset is given with higher magnification

focusing on the basal planes of the anatase nanoparticles. d) Typical HAADF-STEM image of the SiO_2-TiO_2 NCs in a selective area. Elemental mapping for e) O, f) Si and g) Ti.

The crystalline phase of the TiO_2 NPs was identified using Raman spectroscopy. Figure 5 presents the Raman spectra of the plasma-deposited NC thin film (black line) and the TiO_2 NPs spin coated thin films (red line) using the as synthesized colloidal solution, with a focus on the Eg anatase peak. The analysis was limited to using the peak positions since extreme caution is required when using the Raman intensities of very thin films. Raman modes can be assigned to the Raman spectra of the anatase crystal: 144 (Eg), 200 (Eg), 400 (B1g), 513 (A1g), 518 (B1g) and 642 cm^{-1} (Eg) [34,35]. In this figure, it can be observed that the Eg peak lies at 154 cm^{-1}, a value shifted from the expected anatase peak at 144 cm^{-1} [36,37]. It is well-established experimentally that Raman spectra of low-dimensional semiconductor crystals are modified when compared to the one of bulk crystals: (1) the Raman peaks are asymmetrically broadened and (2) their positions are shifted [38,39]. The former is not observed mainly due to the size distribution of the specific nanocrystals. This effect, results in masking the confinement effect and averaging the Raman response [40]. However, the results presented in Figure 5 (black line) confirm the strong shift of the Eg band that the plasma-deposited TiO_2 NPs embedded in the SiO_2 matrix are anatase crystallites and in nanometric size. In addition to this, the Raman spectrum of the TiO_2 NPs thin film through the spin-coated technique is given with red color. The fact that for both cases the anatase peak is found in the same position (154 cm^{-1}) confirms that upon the colloidal solution dilution, the TiO_2 NPs injection and the SiO_2 matrix deposition, the nano crystallite is not affected.

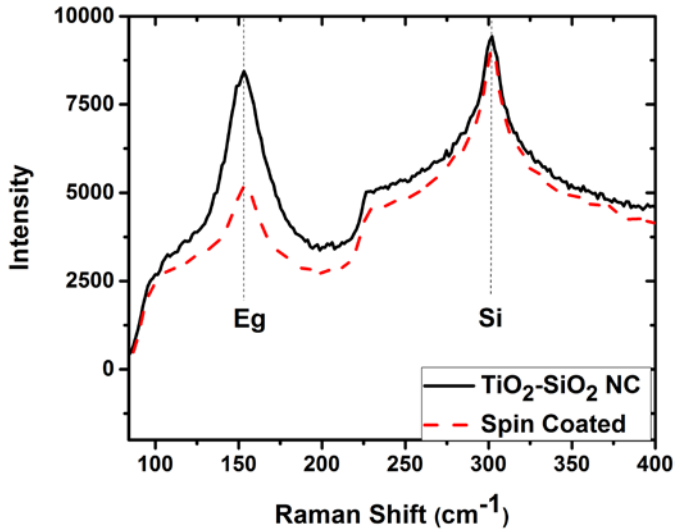

Figure 5: Raman spectra indicating the Anatase Eg band at 154 cm^{-1} and the second order Si band peak at 303 cm^{-1} for the TiO_2-SiO_2 NC thin film through the hybrid approach (black color) and the spin coated TiO_2 NPs thin film using the as synthesized colloidal solution.

3.2 Morphological analysis of the TiO_2-SiO_2 NC thin films

The surface morphological analysis of the TiO_2-SiO_2 NC thin film was investigated by SEM and AFM as shown in Figure 6. From the SEM top view image (Fig. 6a) in high magnification, the surface of the film is homogeneous and nanostructured, revealing some rounded domains. Since the resolution of the SEM is at 10 nm, one can understand that the exact identification and quantification of these domains is impossible. These same rounded domains are highlighted in the AFM measurements (bright yellow-white color in Fig 6b). They are located higher on the z axis and their size is higher than the one of the initial NPs in solution measured by DLS in Figure 1. From detailed analysis of multiple AFM scans at low and high magnification, the mean size of the domains was extracted and plotted as a histogram in Fig 6c. The fitting of a LogNormal distribution provided a mean size of 23 nm of these rounded domains and a standard deviation of 0.3 nm. The Rq (RMS) roughness of the NC film was also deduced. A value of 2 nm was obtained, which was far different from the measured roughness of the silica thin film (Fig. 6c, Rq (RMS) = 0.3 nm) obtained by PECVD with the same reactor in comparable experimental conditions. The AFM scan for this case is given in Figure 6c, revealing the much smoother topography having a Rq (RMS) roughness lower than 5 nm. Since the deposition on flat silicon substrate should not lead to additional roughness or nanostructuration, especially for the deposition of amorphous SiO_2 (matrix), the nanometric pattern observed by AFM must be linked to the presence of TiO_2 NPs inside the SiO_2 matrix. It is worth highlighting, however, that the mean domain size displayed in Figure 6 (23 nm) is much larger than the mean size of TiO_2 NPs obtained from both DLS (Figure 1) and TEM (Figure 4a). This is because TiO_2 NPs are located at different locations across the thickness of the SiO_2 matrix (85 +/- 6 nm) and the PECVD process used in this study provides highly conformal plasma deposition.[41–45] Therefore, the deeper the particle is located inside the matrix, the larger is the size of the structure observed by SEM and AFM on the topmost surface[15,46].

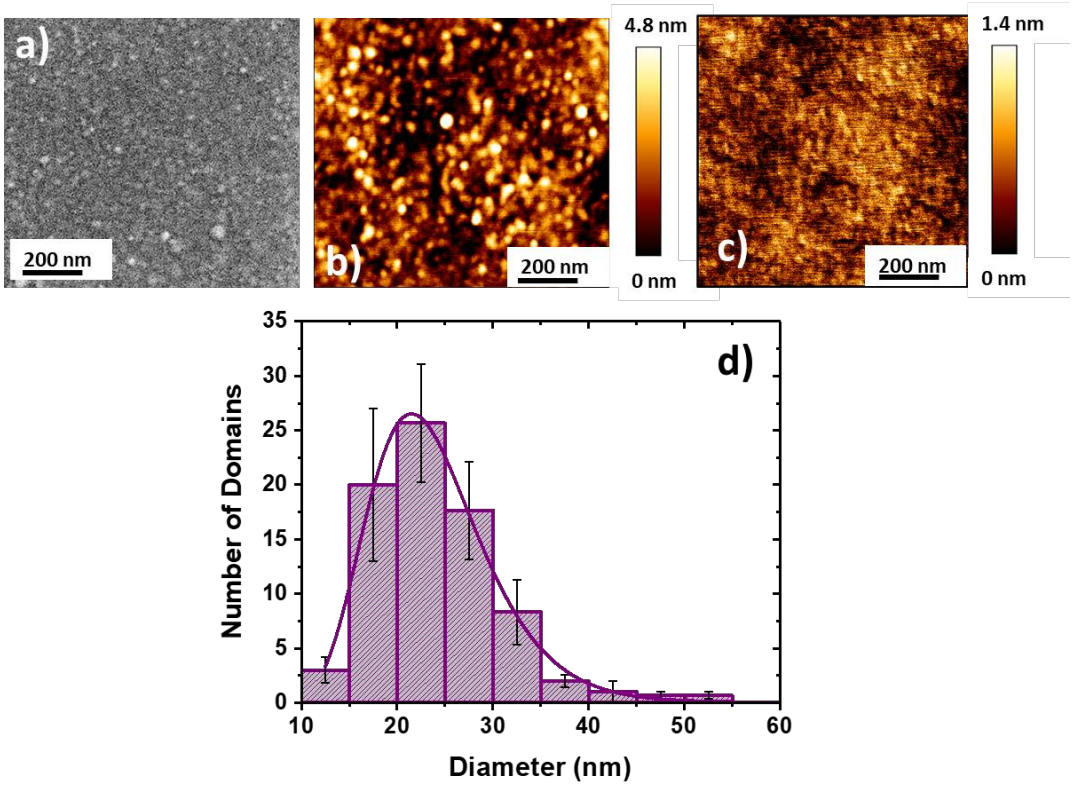

Figure 6: a) SEM secondary electron image of the surface, b) AFM scan (1 µm x 1 µm) of the TiO_2-SiO_2 NC thin films, c) AFM scan (1 µm x 1 µm) of SiO_2 only when deposited on Si substrate and d) size distribution of the rounded domains deduced from the AFM scans.

From the high-magnification and highly-localized analysis obtained both from TEM and SEM/AFM, the plasma-deposited TiO_2-SiO_2 NC thin films indicated a rather homogenous spatial distribution. To have an overall view of this film, low-magnification EDX mappings of the film's surface were recorded. To extract adequate resolution for each element, a thicker film was especially deposited on the ITO/PETsubstrate (224 nm). The results are presented in Figure 7. While homogeneous distributions are observed for silicon and oxygen elements over the 2552 μm^2 surface, abnormal rounded-ring shapes with diameters of several tens of micrometers can be seen for the titanium element. Such feature suggests the well-known coffee-ring effect, happening when the solute migrate in the edge of the evaporating droplet due to the formation of preferential flow and faster evaporation at this area. [47–49] Based on such large-scale SEM and EDX observations, it seems that TiO_2 species are provided to the substrate during growth as droplet and that evaporation and removal of organic species from the solvent[30] occur, at least partially, on the substrate surface rather than in the gas phase.

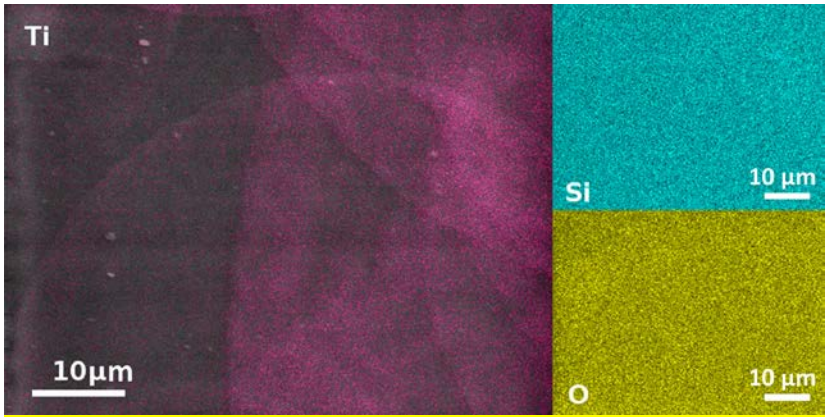

Figure 7: SEM backscattered electrons image and EDX map of Ti superimposed (left) and corresponding EDX maps of Si and O (right).

A quantitative EDX analysis was conducted on the large region (2552 μm^2) avoiding an area exhibiting droplet traces such as the ones shown in Figure 7. In order to avoid all inhomogeneity aspects (in particular those related to the Ti element), only averaged values are shown in Table 1. The results are presented only for Ti and Si due the weak energy of the carbon and oxygen EDX peaks and the strong interactions throughout the layers for these elements (see details in Sec. 2.2). From such analysis, 15% Ti and 85% Si is obtained (atomic %). Based on the calculations provided in the ESI, the volume percentage corresponding to 15 at% is estimated to reach 16 %.

Table 1: Quantitative results by EDX on large surface (2552 μm^2 - magnification X1000).

	Weight %	Atomic %

Silicon	76.9	85
Titanium	23.1	15

3.3 Surface chemical composition investigation of the TiO_2-SiO_2 NC thin films

The chemical analysis of the topmost surface of the TiO_2-SiO_2 NC thin films was carried out with XPS. Four different positions were measured on the same sample. Figure 8 represents the intensity of the O 1s, Ti 2p, C 1s and Si peaks. From these elementary spectra, the mean atomic concentration and the standard deviation in percentage is given by considering the components included in each atomic peak. The contribution of oxygen bonded to silicon atoms, noted as O-Si appears at the binding energy of 532.6 eV whereas the one corresponding to the bond with titanium, noted as O-Ti, at 530.5 eV. [6] A noteworthy observation in this figure is that no peak corresponding to Ti-O-Si (at 531.5 eV [50]) can be found, as expected for a NC, confirming that only two different phases are detected in the film.[50] As reported by many authors [24,51], the signal of titanium element in XPS results from two separated peaks that can be attributed to Ti $_{2p3/2}$ and Ti $_{2p1/2}$. The 2p3/2 peak lies at 458.5 eV as expected for Ti^{4+} cations in TiO_2. Since the injected colloidal solution of TiO_2 NPs was synthesized in an organic solvent, the contribution of carbon element was investigated. Therefore, three components were identified in the C 1s peak. The first and most prominent one, at 285eV, is usually assigned to C-C bonds of both adventitious elemental carbon and the solvent, while the second, at 286.0eV, and the third, 288.5eV, can be related to -C-O bonds and C=O bonds, respectively. Finally, the Si 2p3/2 peak has a binding energy of 103 eV, which is related to the fully oxidized SiO_2 matrix [51]. Consequently, from the Ti2p and Si 2p signals only, the estimated atomic percentage in Ti is at 12 ± 0.004 % and for Si at 88 ± 0.004 %; these values are consistent with those obtained by EDX at the SEM (Table 1). The atomic percentage from XPS can be treated in the same manner as in Section 3.2 and the calculations provided in the ESI, leading to a volume percentage of 13 %.

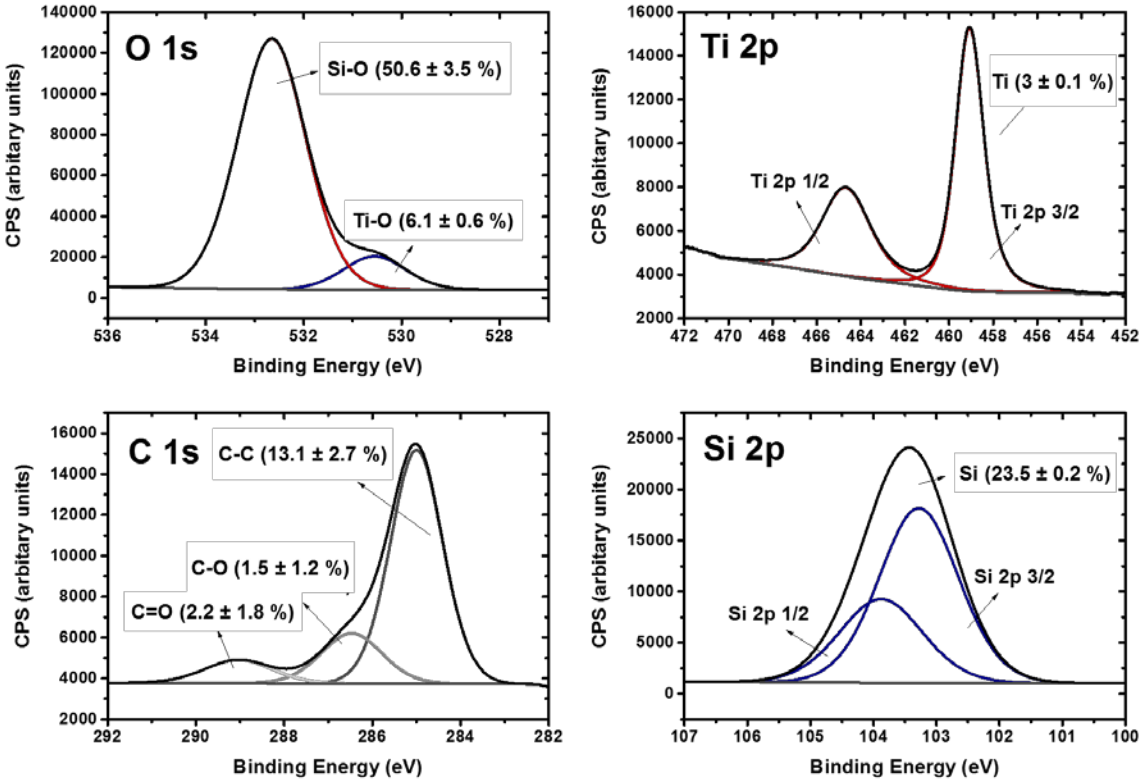

Figure 8: O 1s, Ti 2p, C 1s and Si 2p peaks of the TiO_2-SiO_2 NC thin film measured by XPS (mean atomic percentages and standard deviation of the components from 4 different positions in between brackets).

3.4 Spectroscopic ellipsometry of the TiO_2-SiO_2 NC thin films

The investigation of the optical and physical characteristics was carried out with spectroscopic ellipsometry. The ellipsometric ratio $\rho = \tan(\mathrm{Psi})\exp(j\mathrm{Delta})$ is analyzed from the measured Psi and Delta. To extract the structural and optical information from these data, the sample was modeled as a homogenous layer on silicon substrate, without any top-layer roughness. Due to droplet traces observed at low magnification in the Section 3.1, a more pronounced diffusion of the incident light was observed (in the measurement) at shorter wavelengths. Hence, the fitting was carried out in the limited range of 550 - 1000 nm. The validity of the model and therefore the evaluation of the accuracy of the fit was estimated by the Mean Square Error (MSE) factor. [52]

Assuming the ellipsometry was not sensitive enough to detect the NC nature of the sample, the first ellipsometric model used was a one phase material with Tauc-Lorentz dispersion law (Figure 9a, Model A).[52] However, the experimental and simulated data show discrepancies, providing a high value of the error value (MSE=22). Therefore, a two-phase material (SiO_2 and TiO_2) was set up to account for the ellipsometric data of the TiO_2-SiO_2 NC thin films. First, the dispersion laws for the SiO_2 matrix and the TiO_2 NPs have to be assessed. Conducting an experiment of depositing the SiO_2 matrix while injecting the solvent without the NPs, using the same injection conditions as the plasma-deposited TiO_2-SiO_2 NC thin films, allowed us to acquire a reference SiO_2 matrix film and assess its quality, in the range between 550 and 1000

nm. The model used to fit the ellipsometry data of the matrix was the one of the classical thermal SiO_2 material, as expressed by Herzinger et al. [53] using the Sellmeier/Cauchy dispersion law. The measured and simulated Psi and Delta signals are given in Figure 10a. In this figure, the quality of the fit appears to be high and the MSE for all the wavelength range was given at MSE=10. In Figure 10b, the refractive index (n) and the extinction coefficient (k) of the SiO_2 matrix are given. For the TiO_2 NPs, the Tauc-Lorentz dispersion law was used based on a spin-coated 50 nm TiO_2 NPs film. The effective refractive index for this spin coated film was found at 1.68 at 633 nm wavelength (as voids where evidenced in the film) and the optical bandgap (E_g) at 3.4 eV. The detailed results can be found in a very recent publication of the group.[25] The fit of the NC film using the second model (Model B), resulted in an improved error (MSE=4).

Then, based on the cross-section results obtained with TEM (Fig. 4, Section 3.1) for the nanocomposite film, the Bruggeman Effective Medium Approximation (BEMA) was used (Figure 9b, Model B) to model the TiO_2 NPs dispersed in the SiO_2 matrix. A much better agreement was observed between the experimental and the simulated data.

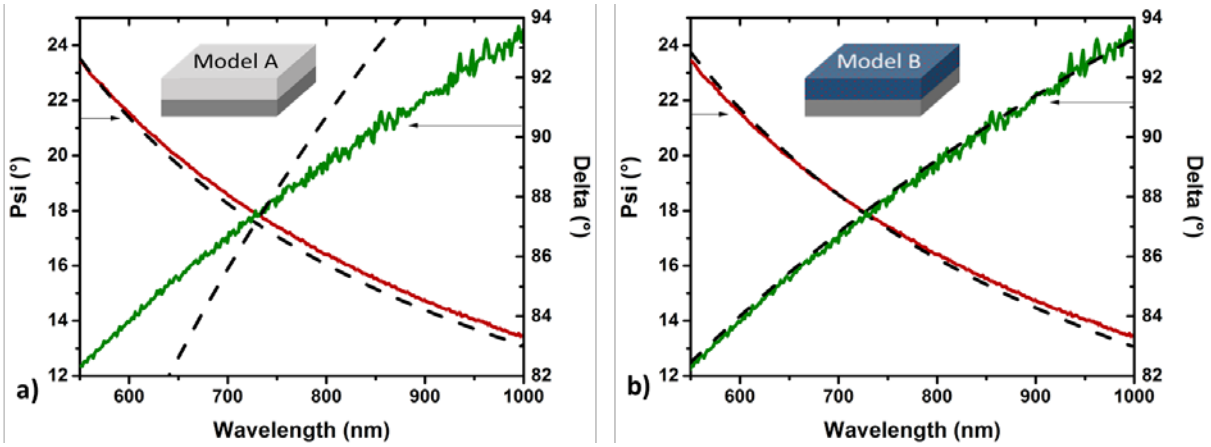

Figure 9: Psi (red) and Delta (green) results of the measured (continuous) and modeled (dashed) data with ellipsometry, based on Model A (a) and Model B (b).

Additionally, from the BEMA, the volume fraction of TiO_2 NPs in the film could be deduced reaching 19 vol.% and 81 vol.% of SiO_2. This observation confirms the EDX and XPS results (Section 3.2), where no mixed (Ti-O-Si) bonding was observed. The optical TiO_2 energy gap is determined at 3.4 eV due to the nanometric size of the TiO_2 [54,55]. In addition, the effective refractive index at 633 nm wavelength was estimated at 1.59, an increased value compared to the SiO_2 matrix itself (1.46).

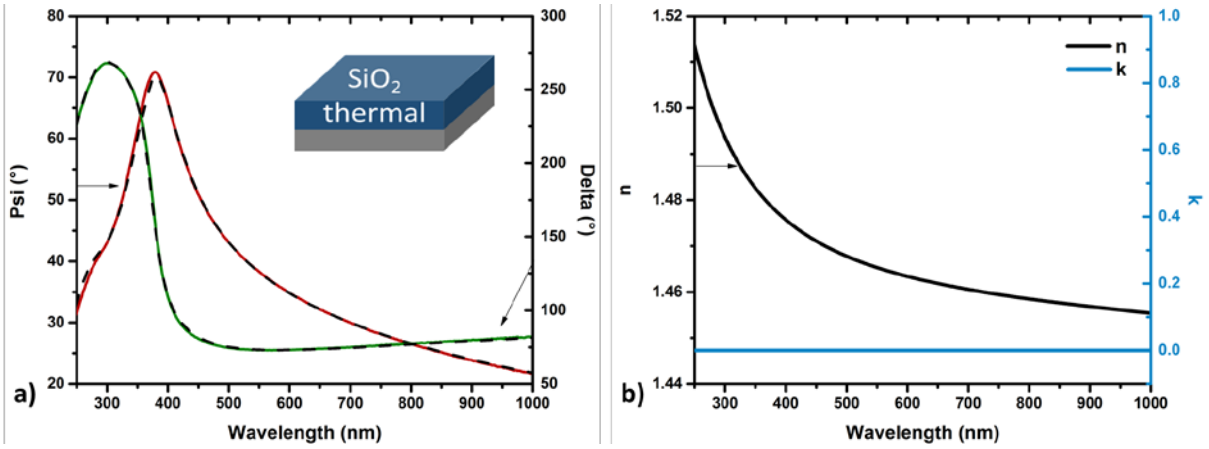

Figure 10: a) Psi (red) and Delta (green) results of the measured (continuous) and modeled (dashed) data with ellipsometry of the matrix only fitted with SiO_2 thermal model.

3.5 Comparison with lower and higher TiO_2 NPs injection rate

To assess the agility of this hybrid process into acquiring NC thin films with different composition and optical characteristics, experiments with lower and higher injection rate were attempted. The N of the injection sequence (for deposition of TiO_2 NPs) was set either at N=2 or at N=30 (instead of 10) and the flow rate of the HMDSO precursor (for deposition of the SiO_2 matrix) was kept at 0.11 sccm. The total deposition time was maintained at 50 min. Figure 11a provides the stacked column (%) resulting from the XPS core level spectra fitting as explained in Section 3.3. In order to assess the reproducibility of the hybrid approach the XPS stacked column provide the mean value and the standard deviation (as error bars) for two to four different experiments in each condition (including the N=10). As expected, for lower N and therefore lower amount of TiO_2 NPs injected in a minute sequence, the atomic percentage of TiO_2 on the surface of the TiO_2-SiO_2 NC thin film was much lower than N=10 (1% for N=2 and 8% for N=10). Additionally, for the highest TiO_2 NPs injection rate (N=30), we can observe a three times higher TiO_2 percentage (25% for N=30) than the N=10. Furthermore, using the data obtained by spectroscopic ellipsometry, and the Model B proposed in Section 3.4, the percentage of the TiO_2 NPs and the effective refractive index of the NC at 633 nm wavelength was obtained (shown in Figure 11b). Once more, to account for the reproducibility of this hybrid process, the results shown in Figure 11b are extracted from four different experiments for each condition. From these results, a clear dependency of the NC's characteristics on the injection parameters is observed. More specifically, for N=0 when no NPs are injected (SiO_2 matrix only) the refractive index is found at 1.47. As we start injecting a low amount of NPs, hence N=2, the NC film contains 7 vol.% of TiO_2 and reveals a refractive index of 1.50. In accordance, for higher injection (N=10), the NC film contains 16 vol.% and reveals an index of 1.54. For N=30, during the one minute sequence, pulses are applied on the injector constantly and consequently no DLI-OFF exists. Hence, this induces a strong pressure variation (from 16 to 20 mTorr) and may produce less stable plasma conductions both the NPs deposition and the silica matrix. Therefore, the significantly higher error bars than the rest conditions could be explained. Nevertheless, for the highest amount of the injected NPs (N=30), the NC film can reach up to 53 vol.% in TiO_2 NPs leading to a refractive index of 1.74.

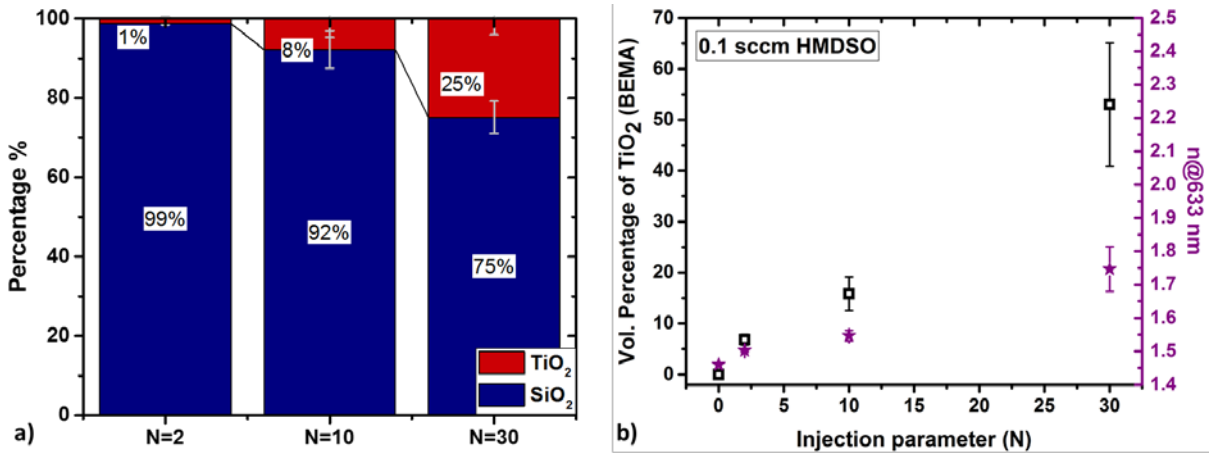

Figure 11: a) Stacked columns (%) of the NC surface composition obtained from XPS for N=2, N=10 and N=30 with measurements obtained from two to four samples. b) Volume percentage of TiO_2 extracted from the BEMA and refractive index at 633 nm wavelength for N=0, N=2,N=10 and N=30 extracted from four samples.

4. Discussion

As demonstrated above, over the range of experimental conditions investigated, the deposition of TiO_2-SiO_2 NC thin films using a hybrid approach leads to small and isolated (non-aggregated) TiO_2 NPs well-distributed into a dense and inorganic SiO_2 matrix. Compared to other processes reported in scientific literature (mostly based on atmospheric-pressure systems)[15,22,46,56,57], the proposed method significantly limits agglomeration of the NPs and improves their dispersion in the matrix. An additional important factor leading to the limited agglomeration of the NPs could be the initially very small size of the NPs in the stable (over time and composition) colloidal solution. Changes in the agglomeration dynamics could partially be attributed to the differences affecting the aerosol formation dynamics between operating at low pressure compared to atmospheric conditions. In particular, at low pressure, the nature of the flow is mainly molecular flow whereas it is laminar or even turbulent at atmospheric pressure. [12,58,59] It could also be related to the low injection rates of the colloidal solution. Using a direct-liquid injection in a CVD system at low pressure, Varvaele et al. [11] have identified that low colloidal solution injection rates (as in this study) promotes the dispersion of the NPs whereas at higher rates, they tend to coalesce such that the mean size distribution shifts towards higher values.

Because of the overall good homogeneity of the film, the optical and dielectric properties of the films could also be deduced by proper modelling of the ellipsometric signals (especially between 550 and 1000 nm). This feature qualifies the process as suitable for the preparation of TiO_2-SiO_2 NC thin film for optical applications in this wavelength range. Despite the solvent injection, the plasma-deposited matrix proved to be of high quality as the fit with thermal silica was significantly accurate. This is a proof that carbon is not incorporated inside the matrix confirming its inorganic nature. By tuning the injection sequence, it was further possible to tune the effective refractive index, having the possibility to reach up to 53 vol% in TiO_2. To the best

of our knowledge, these results are unique compared to the reported approaches. [12,15,22,46,56,60] Due to the set of experimental conditions used, the combination of adjusted volatility of solvents, remarkable stability of the colloidal solution and condition of spraying in a low-pressure plasma reactor resulted in an efficient transport of the droplets containing the non-agglomerated NPs towards the substrate. The optimization of the injection sequence permitted to keep the NPs protected inside the liquid droplets down to the substrate, thus preventing them to aggregate following their interaction with the plasma species. A downside of these liquid droplets as observed by the low magnification SEM-EDX images is the coffee ring patterns of the TiO_2 NPs. Several works report the depiction of droplets due to the limited volatility of the injected solution or the increased mean size (due to system limitations) of the produced droplets [9,61,62]. Given that some of the produced droplets in the specific system (by the direct-liquid injector) do not have enough time to evaporate (low volatility of the solvent), the evaporation process happens at the surface of the film. Further works are under progress to get better insight in the mechanisms involved during the process in terms of droplet formation, droplet travel speed and evaporation of droplet solvents due to the interaction with the low-pressure plasma. This will open a promising chapter for understanding the impact of low-pressure plasma on the physical and chemical state of the liquid droplet during plasma deposition of NC thin films.

5. Conclusion

In this work, the creation of TiO_2-SiO_2 NC thin films by injecting a colloidal solution in a very-low-pressure O_2/HMDSO plasma was reported for the first time. The iterative injection sequence was selected in a way to control and maintain in low levels the deposition rate of the NC films. The pressure was maintained at 3 mTorr (with slight variations) leading to the deposition of good-quality inorganic SiO_2 matrix. The cross section of the film revealed a fairly homogeneous distribution of the NPs inside the matrix, at the local scale. The amount of these 3-nm NPs was evaluated by multiple characterization techniques and was estimated at 16 vol. % at the SEM scale and 19 vol. % as deduced from ellipsometry *i.e.* on a larger area. The surface composition revealed a slightly lower value (13 vol. %), which could be explained due to the coating effect of the SiO_2 matrix (during the last second of the injection sequence). Notably, not significant agglomeration of NPs was observed. Adjusting the parameters of the injection sequence (from N=2 to to N=30), NC films with lower and higher TiO_2 NPs content and thus different optical properties could be achieved. Due to the originality of this work and its novelty, large-surface area deposition has still to be improved. This requires conducting theoretical and further experimental studies to understand the behavior and evaporation of the liquid droplets inside low-pressure plasmas. Through these first results it is evidenced that potentially, an agile approach like this could give the freedom to tune and adjust the NC's properties by adjusting both the nature of the NPs and the matrix but also of the injection parameters reaching a large range of NPs content inside the matrix.

Acknowledgements

Franck Petitgas is thanked for the technical assembly of the reactor and Dr Simon Bulou (LIST) is thanked for his support in conducting PDA measurements. The France-Québec International Research Network on

582 “Nanomatériaux Multifonctionnels Contrôlés” is thanked for the financial support to short-term exchanges
583 between University of Montréal and Institut des Matériaux Jean Rouxel. The CIMEN Electron Microscopy Center
584 in Nantes is greatly acknowledged, for access to TEM funded by the French Contrat Plan État-Région and the
585 European Regional Development Fund of Pays de la Loire. Dr Quentin Hatte is thanked for fruitful discussions
586 regarding image processing.

587 **References**

588 [1] Nelson J K 2010 *Dielectric polymer nanocomposites* (New York: Springer)

589 [2] Guldin S, Kohn P, Stefik M, Song J, Divitini G, Ecarla F, Ducati C, Wiesner U and Steiner
590 U 2013 Self-Cleaning Antireflective Optical Coatings *Nano Lett.* **13** 5329–35

591 [3] Kermadi S, Agoudjil N, Sali S, Zougar L, Boumaour M, Broch L, En Naciri A and Placido
592 F 2015 Microstructure and optical dispersion characterization of nanocomposite sol–gel
593 TiO 2 –SiO 2 thin films with different compositions *Spectrochim. Acta. A. Mol. Biomol.*
594 *Spectrosc.* **145** 145–54

595 [4] Charitidis C A, Georgiou P, Koklioti M A, Trompeta A-F and Markakis V 2014
596 Manufacturing nanomaterials: from research to industry *Manuf. Rev.* **1** 11

597 [5] Larouche S, Szymanowski H, Klemberg-Sapieha J E, Martinu L and Gujrathi S C 2004
598 Microstructure of plasma-deposited SiO2/TiO2 optical films *J. Vac. Sci. Technol. Vac.*
599 *Surf. Films* **22** 1200–7

600 [6] Li D, Elisabeth S, Granier A, Carette M, Goullet A and Landesman J-P 2016 Structural
601 and Optical Properties of PECVD TiO $_2$ -SiO $_2$ Mixed Oxide Films for Optical
602 Applications: Structural and Optical Properties of PECVD TiO $_2$ -SiO $_2$ … *Plasma*
603 *Process. Polym.* **13** 918–28

604 [7] Nedfors N, Tengstrand O, Flink A, Andersson A M, Eklund P, Hultman L and Jansson U
605 2014 Reactive sputtering of NbCx-based nanocomposite coatings: An up-scaling study
606 *Surf. Coat. Technol.* **253** 100–8

607 [8] Profili J, Levasseur O, Koronai A, Stafford L and Gherardi N 2017 Deposition of
608 nanocomposite coatings on wood using cold discharges at atmospheric pressure *Surf.*
609 *Coat. Technol.* **309** 729–37

610 [9] Ross A D and Gleason K K 2006 The CVD of Nanocomposites Fabricated via Ultrasonic
611 Atomization *Chem. Vap. Depos.* **12** 225–30

612 [10] Carnide G Procédé de préparation de nanoparticules

613 [11] Vervaele M, De Roo B, Deschaume O, Rajala M, Guillon H, Sousa M, Bartic C, Van
614 Haesendonck C, Seo J W and Locquet J-P 2016 Development of a new direct liquid
615 injection system for nanoparticle deposition by chemical vapor deposition using
616 nanoparticle solutions *Rev. Sci. Instrum.* **87** 025101

617 [12] Ogawa D, Saraf I, Sra A, Timmons R, Goeckner M and Overzet L 2009 The direct
618 injection of liquid droplets into low pressure plasmas *J. Vac. Sci. Technol. Vac. Surf. Films*
619 **27** 342–51

[13] Fanelli F, Mastrangelo A M and Fracassi F 2014 Aerosol-Assisted Atmospheric Cold Plasma Deposition and Characterization of Superhydrophobic Organic–Inorganic Nanocomposite Thin Films *Langmuir* **30** 857–65

[14] Bruggeman P J, Kushner M J, Locke B R, Gardeniers J G E, Graham W G, Graves D B, Hofman-Caris R C H M, Maric D, Reid J P, Ceriani E, Fernandez Rivas D, Foster J E, Garrick S C, Gorbanev Y, Hamaguchi S, Iza F, Jablonowski H, Klimova E, Kolb J, Krcma F, Lukes P, Machala Z, Marinov I, Mariotti D, Mededovic Thagard S, Minakata D, Neyts E C, Pawlat J, Petrovic Z L, Pflieger R, Reuter S, Schram D C, Schröter S, Shiraiwa M, Tarabová B, Tsai P A, Verlet J R R, von Woedtke T, Wilson K R, Yasui K and Zvereva G 2016 Plasma–liquid interactions: a review and roadmap *Plasma Sources Sci. Technol.* **25** 053002

[15] Profili J, Levasseur O, Blaisot J-B, Koronai A, Stafford L and Gherardi N 2016 Nebulization of Nanocolloidal Suspensions for the Growth of Nanocomposite Coatings in Dielectric Barrier Discharges: Nebulization of Nanocolloidal Suspensions… *Plasma Process. Polym.* **13** 981–9

[16] Dembele A, Rahman M, Reid I, Twomey B, MacElroy J M D and Dowling D P 2011 Deposition of Hybrid Organic–Inorganic Composite Coatings Using an Atmospheric Plasma Jet System *J. Nanosci. Nanotechnol.* **11** 8730–7

[17] Bardon J, Bour J, Del Frari D, Arnoult C and Ruch D 2009 Dispersion of Cerium-Based Nanoparticles in an Organosilicon Plasma Polymerized Coating: Effect on Corrosion Protection *Plasma Process. Polym.* **6** S655–9

[18] Del Frari D, Bour J, Bardon J, Buchheit O, Arnoult C and Ruch D 2010 Hybrid Layers Deposited by an Atmospheric Pressure Plasma Process for Corrosion Protection of Galvanized Steel *J. Nanosci. Nanotechnol.* **10** 2611–9

[19] Avril L, Boudon J, Marco de Lucas M C and Imhoff L 2014 Alumina particle reinforced TiO2 composite films grown by direct liquid injection MOCVD *Vacuum* **107** 259–63

[20] Profili J, Levasseur O, Naudé N, Chaneac C, Stafford L and Gherardi N 2016 Influence of the voltage waveform during nanocomposite layer deposition by aerosol-assisted atmospheric pressure Townsend discharge *J. Appl. Phys.* **120** 053302

[21] Profili J, Levasseur O, Koronai A, Stafford L and Gherardi N 2017 Deposition of nanocomposite coatings on wood using cold discharges at atmospheric pressure *Surf. Coat. Technol.* **309** 729–37

[22] Brunet P, Rincón R, Martinez J-M, Matouk Z, Fanelli F, Chaker M and Massines F 2017 Control of composite thin film made in an Ar/isopropanol/TiO2 nanoparticles dielectric barrier discharge by the excitation frequency *Plasma Process. Polym.* n/a-n/a

[23] Karpinski A, Berson S, Terrisse H, Mancini-Le Granvalet M, Guillerez S, Brohan L and Richard-Plouet M 2013 Anatase colloidal solutions suitable for inkjet printing: Enhancing lifetime of hybrid organic solar cells *Sol. Energy Mater. Sol. Cells* **116** 27–33

[24] El Kass M, Brohan L, Gautier N, Béchu S, David C, Lemaitre N, Berson S and Richard-Plouet M 2017 TiO_2 Anatase Solutions for Electron Transporting Layers in Organic Photovoltaic Cells *ChemPhysChem* **18** 2390–6

[25] Mitronika M, Profili J, Goullet A, Stafford L, Granier A and Richard-Plouet M 2020 Modification of the optical properties and nano-crystallinity of anatase TiO2nanoparticles thin film using low pressure O2 plasma treatment *Thin Solid Films* **709** 138212

[26] Nicolazo F, Goullet A, Granier A, Vallee C, Turban G and Grolleau B 1998 Study of oxygen/TEOS plasmas and thin SiOx films obtained in an helicon diffusion reactor *Surf. Coat. Technol.* **98** 1578–1583

[27] Granier A, Nicolazo F, Vallée C, Goullet A, Turban G and Grolleau B 1997 Diagnostics in helicon plasmas for deposition *Plasma Sources Sci. Technol.* **6** 147–56

[28] Kooij S, Sijs R, Denn M M, Villermaux E and Bonn D 2018 What Determines the Drop Size in Sprays? *Phys. Rev. X* **8**

[29] Bousquet A, Bursikova V, Goullet A, Djouadi A, Zajickova L and Granier A 2006 Comparison of structure and mechanical properties of SiO2-like films deposited in O2/HMDSO pulsed and continuous plasmas *Surf. Coat. Technol.* **200** 6517–21

[30] Mitronika M, Profili J, Goullet A, Stafford L, Granier A and Richard-Plouet M 2020 Modification of the optical properties and nano-crystallinity of anatase TiO2nanoparticles thin film using low pressure O2 plasma treatment *Thin Solid Films* **709** 138212

[31] Pouchou J-L 2002 X-Ray Microanalysis of Thin Surface Films and Coatings *Microchim. Acta* **138** 133–52

[32] Christien F, Ferchaud E, Nowakowski P and Allart M 2012 The Use of Electron Probe MicroAnalysis to Determine the Thickness of Thin Films in Materials Science *X-Ray Spectroscopy* ed S K Sharma (InTech)

[33] Neal Fairley 2005 *Copyright© 2005 Casa Software Ltd*

[34] Zhang W F, He Y L, Zhang M S, Yin Z and Chen Q 2000 Raman scattering study on anatase TiO $_2$ nanocrystals *J. Phys. Appl. Phys.* **33** 912–6

[35] Ohsaka T, Izumi F and Fujiki Y 1978 Raman spectrum of anatase, TiO2 *J. Raman Spectrosc.* **7** 321–4

[36] Ma W, Lu Z and Zhang M 1998 Investigation of structural transformations in nanophase titanium dioxide by Raman spectroscopy *Appl. Phys. Mater. Sci. Process.* **66** 621–7

[37] Pighini C, Aymes D, Millot N and Saviot* L 2007 Low-frequency Raman characterization of size-controlled anatase TiO2 nanopowders prepared by continuous hydrothermal syntheses *J. Nanoparticle Res.* **9** 309–15

[38] Gao Y, Zhao X, Yin P and Gao F 2016 Size-Dependent Raman Shifts for nanocrystals *Sci. Rep.* **6**

[39] Rolo A G and Vasilevskiy M I 2007 Raman spectroscopy of optical phonons confined in semiconductor quantum dots and nanocrystals *J. Raman Spectrosc.* **38** 618–33

[40] Kelly S, Pollak F H and Tomkiewicz M 1997 Raman Spectroscopy as a Morphological Probe for TiO $_2$ Aerogels *J. Phys. Chem. B* **101** 2730–4

[41] Raupp G B, Levedakis D A and Cale T S 1995 Conformality of SiO_2 films from tetraethoxysilane-sourced remote microwave plasma-enhanced chemical vapor deposition *J. Vac. Sci. Technol. Vac. Surf. Films* **13** 676–80

[42] Park M, Yu H K, Koo J G, Jang J and Nam K S 1998 High-quality conformal silicon oxide films prepared by multi-step sputtering PECVD and chemical mechanical polishing *J. Electron. Mater.* **27** 1262–7

[43] Savin de Larclause I, Paulmier T, Enache I, Caquineau H, Raynaud P, Massines F and Gherardi N 2009 Conformity of Silica-like Thin Films Deposited by Atmospheric Pressure Townsend Discharge and Transport Mechanisms *IEEE Trans. Plasma Sci.* **37** 970–8

[44] Sobel N, Hess C, Lukas M, Spende A, Stühn B, Toimil-Molares M E and Trautmann C 2015 Conformal SiO_2 coating of sub-100 nm diameter channels of polycarbonate etched ion-track channels by atomic layer deposition *Beilstein J. Nanotechnol.* **6** 472–9

[45] Arts K, Utriainen M, Puurunen R L, Kessels W M M and Knoops H C M 2019 Film Conformality and Extracted Recombination Probabilities of O Atoms during Plasma-Assisted Atomic Layer Deposition of SiO_2, TiO_2, Al_2O_3, and HfO_2 *J. Phys. Chem. C* **123** 27030–5

[46] Profili J, Levasseur O, Naudé N, Chaneac C, Stafford L and Gherardi N 2016 Influence of the voltage waveform during nanocomposite layer deposition by aerosol-assisted atmospheric pressure Townsend discharge *J. Appl. Phys.* **120** 053302

[47] Deegan R D, Bakajin O, Dupont T F, Huber G, Nagel S R and Witten T A 1997 Capillary flow as the cause of ring stains from dried liquid drops *Nature* **389** 827–9

[48] Maki K L and Kumar S 2011 Fast Evaporation of Spreading Droplets of Colloidal Suspensions *Langmuir* **27** 11347–63

[49] Yunker P J, Still T, Lohr M A and Yodh A G 2011 Suppression of the coffee-ring effect by shape-dependent capillary interactions *Nature* **476** 308–11

[50] Ondračka P, Nečas D, Carette M, Elisabeth S, Holec D, Granier A, Goullet A, Zajíčková L and Richard-Plouet M 2020 Unravelling local environments in mixed TiO2–SiO2 thin films by XPS and ab initio calculations *Appl. Surf. Sci.* **510** 145056

[51] Moulder J F, Stickle W F, Sobol P E, Bomben K D, Chastain J, King Jr. R C and Physical Electronics, Incorporation 1995 *Handbook of X-ray photoelectron spectroscopy: a reference book of standard spectra for identification and interpretation of XPS data* (Eden Prairie, Minn.: Physical Electronics)

[52] Saha D, Ajimsha R S, Rajiv K, Mukherjee C, Gupta M, Misra P and Kukreja L M 2014 Spectroscopic ellipsometry characterization of amorphous and crystalline TiO 2 thin films grown by atomic layer deposition at different temperatures *Appl. Surf. Sci.* **315** 116–23

[53] Herzinger C M, Johs B, McGahan W A, Woollam J A and Paulson W 1998 Ellipsometric determination of optical constants for silicon and thermally grown silicon dioxide via a multi-sample, multi-wavelength, multi-angle investigation *J. Appl. Phys.* **83** 3323–36

[54] Gupta S M and Tripathi M 2011 A review of TiO2 nanoparticles *Chin. Sci. Bull.* **56** 1639–57

[55] Enright B and Fitzmaurice D 1996 Spectroscopic Determination of Electron and Hole Effective Masses in a Nanocrystalline Semiconductor Film *J. Phys. Chem.* **100** 1027–35

[56] Profili J, Dap S, Levasseur O, Naude N, Belinger A, Stafford L and Gherardi N 2017 Interaction of atomized colloid with an ac electric field in a dielectric barrier discharge reactor used for deposition of nanocomposite coatings *J. Phys. Appl. Phys.* **50** 075201

[57] Denis D P, Barry T and Gerry B 2010 Effect of Titanium Oxide Nanoparticle Incorporation into nm Thick Coatings Deposited Using an Atmospheric Pressure Plasma *J. Nanosci. Nanotechnol.* **10** 2746–52

[58] Reist P C 1993 *Aerosol science and technology* (New York: McGraw Hill)

[59] Hinds W C 1999 *Aerosol technology: properties, behavior, and measurement of airborne particles* (New York: Wiley)

[60] De Vietro N, Conte A, Incoronato A L, Del Nobile M A and Fracassi F 2017 Aerosol-assisted low pressure plasma deposition of antimicrobial hybrid organic-inorganic Cu-composite thin films for food packaging applications *Innov. Food Sci. Emerg. Technol.* **41** 130–4

[61] Goeckner M, Ogawa D, Saraf I and Overzet L 2009 Progress report: Direct injection of liquids into low-pressure plasmas *J. Phys. Conf. Ser.* **162** 012014

[62] Mauchauffé R, Moreno-Couranjou M, Boscher N D, Duwez A-S and Choquet P 2016 Liquid-Assisted Plasma-Enhanced Chemical Vapor Deposition of Catechol and Quinone-Functionalized Coatings: Insights into the Surface Chemistry and Morphology: Liquid-Assisted Plasma-Enhanced Chemical Vapor Deposition of Catechol… *Plasma Process. Polym.* **13** 843–56